Assiut University Journal of Multidisciplinary Scientific Research (AUNJMSR)
Faculty of Science, Assiut University, Assiut, Egypt.
Printed ISSN 2812-5029
Online ISSN 2812-5037
Vol. 54 (3): 452- 468 (2025)
https://aunj.journals.ekb.eg

Synthesis of Ni@Ce-UiO-66 nano catalyst for the production of hydrogen via hydrolysis of sodium borohydride

Ahmed Abdo Hassan[1*], Mostafa Farrag[1], R. M. Gabr[1]

[1]Chemistry Department, Faculty of Science, Assiut University, Assiut, 71516 Egypt
[*] Corresponding author: ahmed_abdo@aun.edu.eg

ARTICLE INFO

Article History:
Received:2025-05-29
Accepted:2025-06-25
Online: 2025-08-28

Keywords:
MOFs,
Ni@Ce-UiO-66,
Sodium borohydride hydrolysis,
Hydrogen,
Catalysis.
.

ABSTRACT

Hydrogen gas (H_2) is commonly regarded as an eco-friendly and renewable energy carrier. Ce-UiO-66 was modified through the impregnation of different concentrations of nickel nitrate ($Ni(NO_3)_2 \cdot 6H_2O$) in order to synthesize such high-performance catalysts, then the catalysts were characterized via XRD, FTIR, and N_2 adsorption techniques. The dehydrogenation of $NaBH_4$ was used to assess the catalytic activity of the synthesized materials. The hydrogen generation rate (HGR) measurements revealed the impact of Ni^{2+} doping. A marked increase in catalytic activity was observed compared to Ce-UiO-66. The work discussed the effects of catalyst loading, $NaBH_4$ concentration, and reaction temperature. 20% Ni@Ce-UiO-66 catalyst demonstrates high (HGR) of 694 $mL \cdot min^{-1} \cdot g^{-1}$. Comprehensive kinetic and thermodynamic evaluations were performed through examining reaction rates (k), activation energy (Ea), and thermodynamic parameters (ΔH, ΔS, and ΔG). The obtained results highlight that these catalysts have strong potential for driving innovations in hydrogen energy systems. Moreover, the results proved high reusability, sustaining consistent performance across four cycles.

INTRODUCTION

The overreliance on fossil fuels, coupled with increasing environmental concerns, has spurred significant research efforts into renewable energy alternatives to replace conventional carbon-based fuels. Among these, hydrogen energy has gained prominence as a leading contender in the clean energy sector, owing to its exceptional energy density and minimal environmental impact advantages that set it apart from traditional fossil fuels. This underscores hydrogen's vital role in both modern industry and everyday applications [1-3]. Currently, numerous production methods exist to generate hydrogen efficiently such as water electrolysis [4], photoelectrolysis [5], thermolysis [6], biological processes [7] and thermochemical conversion methods [8]. More recently, chemical hydrolysis of hydrides, particularly sodium borohydride ($NaBH_4$), has gained widespread adoption as an efficient means of hydrogen generation [9,10]. $NaBH_4$ exhibits

exceptional hydrogen storage capacity (10.8 wt%) and produces non-toxic byproducts through aqueous reactions. Its complete insensitivity to external magnetic fields makes it an outstanding candidate for metallic catalysis, demonstrating both high efficiency and excellent reusability [11]. Remarkably, it enables hydrogen production even under low-temperature conditions. The hydrolysis of $NaBH_4$ yields only environmentally benign byproducts - sodium metaborate ($NaBO_2$) and water - further enhancing its sustainability credentials.

$$\mathbf{NaBH_4+2H_2O \rightarrow 4H_2+NaBO_2} \qquad \mathbf{\Delta H= -212.1\ kJ/mol} \qquad \mathbf{(1)}$$

Heterogeneous catalysts have demonstrated excellent controllability in hydrogen generation processes. Noble metal catalysts, particularly ruthenium (Ru), rhodium (Rh), platinum (Pt), and palladium (Pd), exhibit superior performance in the catalytic hydrolysis of $NaBH_4$. These materials are preferred due to their exceptional catalytic activity, remarkable stability, and strong resistance to deactivation [12-14]. The exorbitant cost and restricted supply of noble metals have driven extensive investigations into developing high-performance catalysts derived from abundant first raw transition metals such as nickel (Ni), iron (Fe), cobalt (Co), and copper (Cu) as cost-effective and abundant substitutes for precious metal catalysts. These non-noble catalysts have been engineered in various forms (e.g., nanoparticles, alloys, and supported composites) to enhance their catalytic efficiency and practical applicability in $NaBH_4$ hydrolysis [15-22]. The catalytic performance of transition metals can be significantly improved by immobilizing them on suitable support materials. Without proper stabilization, transition metal nanoparticles tend to coalesce during catalytic reactions, leading to reduced surface area and diminished catalytic efficiency. Among the various support materials available, metal-organic frameworks (MOFs) have emerged as one of the most promising substrates for anchoring transition metal nanoparticles. MOFs are a class of highly porous, crystalline materials composed of metal ions or clusters coordinated with organic linkers. They have numerous benefits such as a large surface area, low density, substantial pore volume, and various crystal structures [23-28].

Herein, Ni@Ce-UiO-66 catalysts were synthesized through a wet impregnation method, where controlled amounts of nickel nitrate hexahydrate ($Ni(NO_3)_2 \cdot 6H_2O$) were incorporated into the Ce-UiO-66 matrix to optimize its catalytic efficiency for $NaBH_4$ dehydrogenation. Systematic evaluation of hydrogen evolution rates demonstrated that Ni^{2+} incorporation substantially enhanced the dehydrogenation kinetics relative to the pristine Ce-UiO-66 framework. Notably, Ni@Ce-UiO-66 catalysts exhibit substantially enhanced HGR values compared to Ce-UiO-66, highlighting the crucial role of nickel incorporation in boosting dehydrogenation kinetics.

MATERIALS AND METHOD

1. Materials

1.1 Synthesis of Ce-UiO-66

Ce-UiO-66 was synthesized by first dissolving 1.64 g of cerium ammonium nitrate in 3.6 mL water and 0.33 g of terephthalic acid (BDC) in 15.4 mL DMF separately, then gradually adding the BDC solution to the cerium solution under stirring, which produced a yellow precipitate. The mixture was stirred continuously for 24 h at room temperature before the resulting solid was isolated by centrifugation, washed sequentially with DMF and acetone, and finally dried overnight at 80°C [29].

1.2. Synthesis of x% Ni@Ce-UiO-66

Ni@Ce-UiO-66 was synthesized through a wet impregnation method [30]. Briefly, 1 g of the metal-organic framework (MOF) was dispersed in an aqueous solution of nickel nitrate hexahydrate ($Ni(NO_3)_2 \cdot 6H_2O$) with target loadings of 10 and 20 wt.%. The suspension was continuously stirred at 70°C for 2 h, then oven-dried at 100°C for 24 h to obtain the final catalyst.

2. Characterization techniques

Ce-UiO-66 and 20% Ni@Ce-UiO-66 were characterized using complementary analytical techniques. XRD analysis was performed on a Philips PW 2103/100 diffractometer (Cu Kα radiation, λ = 1.5418 Å) with a 5-70° 2θ range at 0.06°/min scanning rate. FTIR spectra (4000-400 cm^{-1}) were acquired at 4 cm^{-1} resolution using a Shimadzu IR-470 spectrophotometer, with samples dispersed in KBr pellets. Textural properties were evaluated through N_2 physisorption at 77 °K using a Quantachrome 3200 system, where approximately 0.1 g samples were degassed prior to BET surface area measurements.

3. $NaBH_4$ hydrolysis

The hydrolysis of $NaBH_4$ was carried out in a 100 mL flask under controlled isothermal conditions (30–50 °C). Hydrogen evolution (V_{H_2}, mL) was monitored gasometrically by measuring water displacement in a calibrated burette, maintaining system pressure equilibrium. The reaction mixture (50 mL of 0.03–0.11 *M* $NaBH_4$) was stirred magnetically to ensure temperature uniformity, and hydrolysis was initiated by adding catalyst (0.03–0.09 g). Before testing, catalysts were pre-activated at 80–100 °C for 1 h. The hydrogen generation rate (HGR) was determined based on the equation:

$$HGR = V_{H_2}(mL) / (t(min) \times m(g))$$

where m is the catalyst mass, t is the time needed for the complete reaction of hydrolytic dehydrogenation, and V_{H_2} is total H_2 produced.

RESULTS AND DISCUSSION

1. Characterization

1.1. XRD analysis

As shown in Fig.1, the x-ray diffractogram of Ce-UiO-66 reveals characteristic reflections at 2θ = 7.4°, 8.5°, 12.0°, 16.5°, 18.0°, and 25.0°, consistent with the cubic framework topology of UiO-66. Minor peak displacements relative to Ce-UiO-66 confirm successful isoreticular substitution with cerium, while peak broadening suggests reduced crystallinity or nanoscale domain formation. Phase purity is evidenced by the absence of extraneous diffraction features. Remarkably, Ni-functionalized Ce-UiO-66 (Ni@Ce-UiO-66) maintains the parental diffraction peaks, indicating preservation of crystallinity with Ni^{2+} incorporation. The invariant lattice parameters and unaltered peak profiles suggest atomic-level dispersion of Ni^{2+} species, likely occupying coordinative unsaturated sites as amorphous moieties within the porous architecture**.**

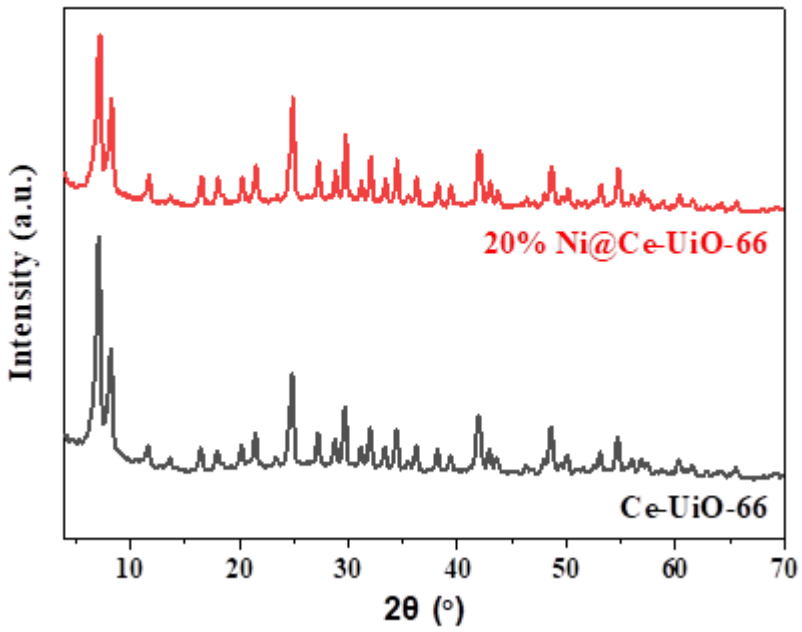

Fig. 1: XRD diffractograms for Ce-UiO-66 and 20% Ni@Ce-UiO-66 catalysts.

1.2. FTIR analysis

To evaluate their chemical compositions, FTIR spectra of Ce-UiO-66 and 20% Ni@Ce-UiO-66 catalysts were recorded and are show in (Fig. 2). Ce-UiO-66 exhibited distinct vibrational bands: O–H stretch (3405 cm^{-1}), C=O stretch (1652 cm^{-1}), aromatic C=C stretch (1500 cm^{-1}), and carboxylate asymmetric/symmetric stretches at 1554 cm^{-1} and 1382 cm^{-1}, respectively [31–36]. Upon Ni^{2+} loading, the O–H band in Ni@Ce-UiO-66 broadened slightly (3380 cm^{-1}), attributed to coordinated water or hydroxyl species from $Ni(NO_3)_2 \cdot 6H_2O$. Notably, the carboxylate peaks shifted to 1560 cm^{-1} (asymmetric) and 1378 cm^{-1} (symmetric), signifying Ni^{2+} coordination with the linker. These observations confirm the successful embedding of nickel ions while maintaining the MOF's structural integrity.

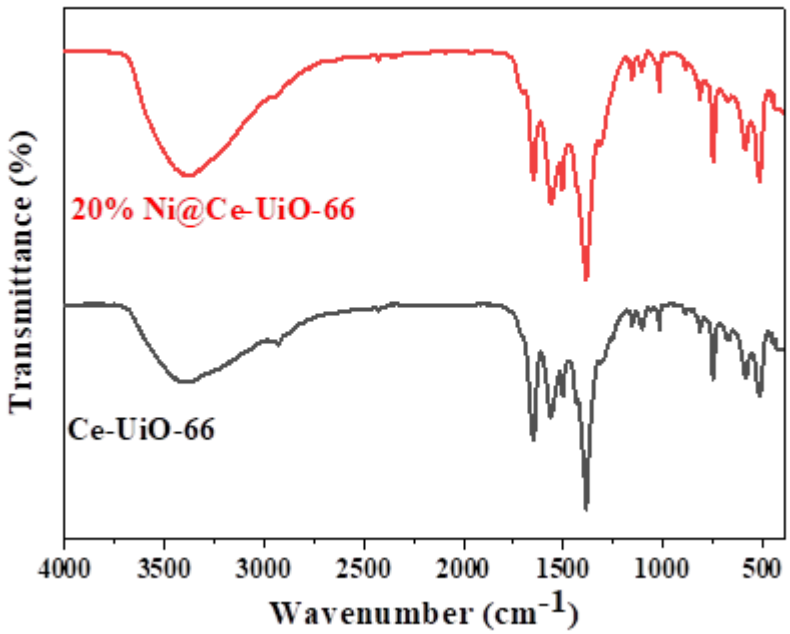

Fig. 2: FT-IR spectra for Ce-UiO-66 and 20% Ni@Ce-UiO-66 catalysts.

1.3. N_2 adsorption

The texture and porosity of Ce-UiO-66 and 20% Ni@Ce-UiO-66 catalysts were studied by analyzing nitrogen adsorption-desorption isotherms (Fig. 3). The adsorption isotherms of the two catalysts were belong to type II isotherms according to Brunauer's classification, accompanied by H4 hysteresis loops, indicating the presence of narrow, uniformly sized pores. The BET surface areas, calculated from adsorption data in the relative pressure range (P/P_0 = 0.05–0.30), were found to be 99.6 and 154 $m^2\ g^{-1}$ for Ce-UiO-66 and 20% Ni@Ce-UiO-66, respectively (Table 1). Pore-size distribution curves

(Fig. 3b) and structural parameters (Table 1) further reveal that the total pore volumes are 3.7 and 5.6 (cc/g) $\times 10^{-2}$, while the average pore diameters are 17.3 and 17.4 Å for Ce-UiO-66 and 20% Ni@Ce-UiO-66, respectively. These findings confirm the microporous nature of both materials, with Ni incorporation enhancing surface area and pore volume.

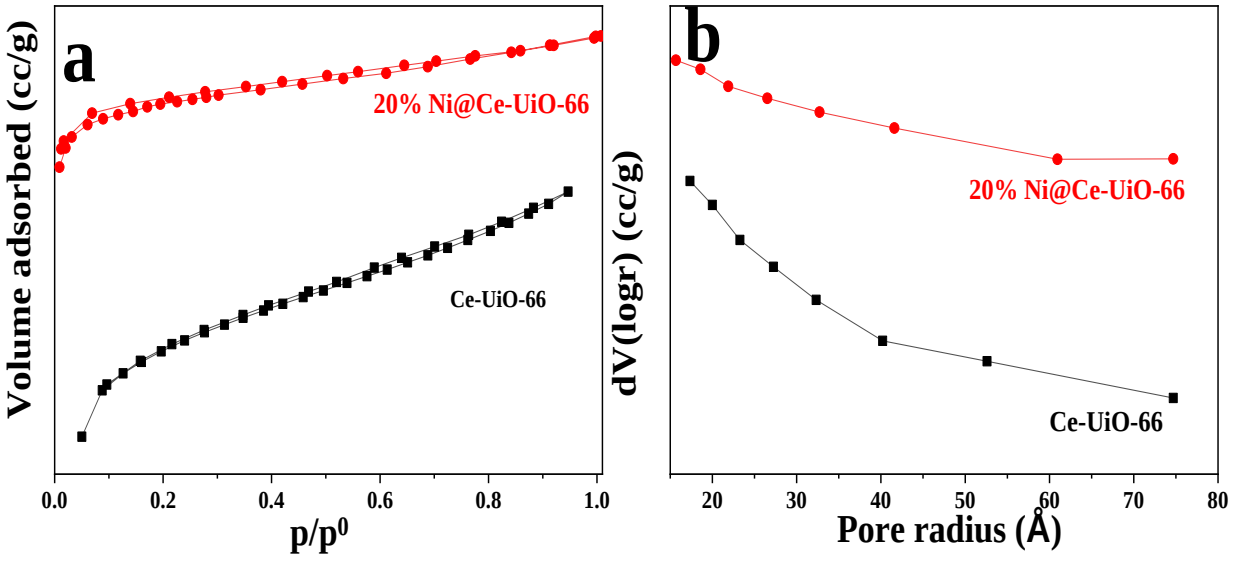

Fig. 3: a) N_2 adsorption-desorption isotherms Ce-UiO-66 and 20% Ni@Ce-UiO-66, b) Pore-size distribution for Ce-UiO-66 and 20% Ni@Ce-UiO-66.

Table (1): The specific surface area S_{BET}, pore characteristics of Ce-UiO-66 and 20% Ni@Ce-UiO-66.

Catalyst	Surface area (S_{BET}) (m^2/g)	Pore volume (cc/g) $\times 10^{-2}$	Pore diameter (Å)
Ce-UiO-66	99.6	3.7	17.3
20% Ni@Ce-UiO-66	154	5.6	17.4

2. Catalytic activity

In order to check the modification of Ce-UiO-66 through the incorporation of Ni^{2+} ions at varying concentrations, preliminary experiments were carried out using sodium borohydride dehydrogenation as a test reaction. As depicted in Fig. 4, the

resulting histogram demonstrates a significant decrease in the time needed to generate 75 mL of H_2, confirming the pronounced influence of Ni^{2+} ions on accelerating the hydrolysis process.

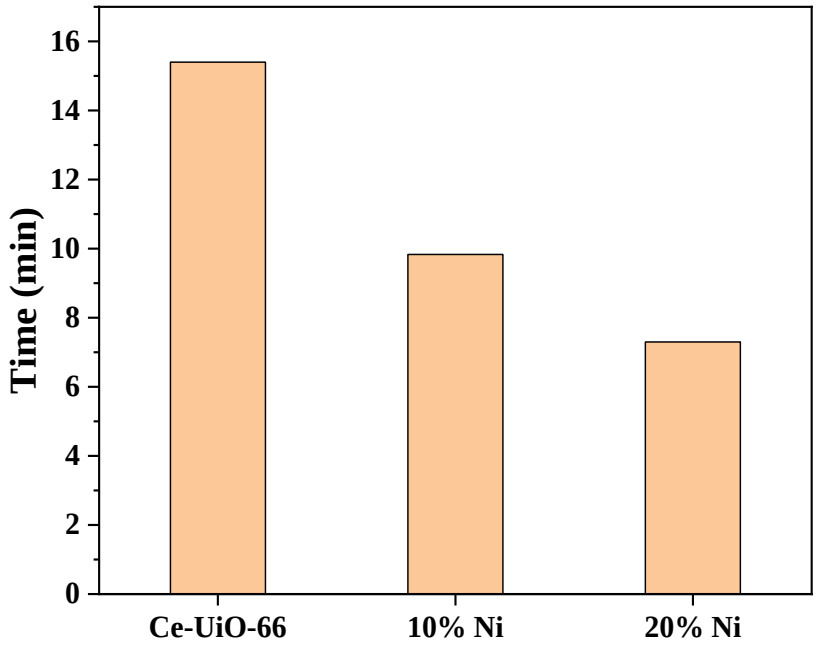

Fig.4: The effect of the Ni loading level (10, 20 wt.%) on the reaction time for V_{75} of hydrogen generated on Ce –UiO-66.

In addition to the significant influence of reaction temperature on the hydrogen generation process, other impacts such as catalyst dose and $NaBH_4$ concentration also play a crucial role in determining both the reaction rate and its kinetic behavior.

2.1. Effect of catalyst weight

The reaction rate is highly dependent on catalyst dosage, as it directly influenced by the available active surface area for the reaction. To explore this relationship, experiments were conducted using various catalyst masses (0.03, 0.05, 0.07, and 0.09 g) using 0.05 *M* $NaBH_4$ at 30 °C. As depicted in Fig. 5, increasing the catalyst dosage significantly reduced the time required to generate 75 mL of H_2, demonstrating a clear correlation between catalyst quantity and reaction efficiency**.**

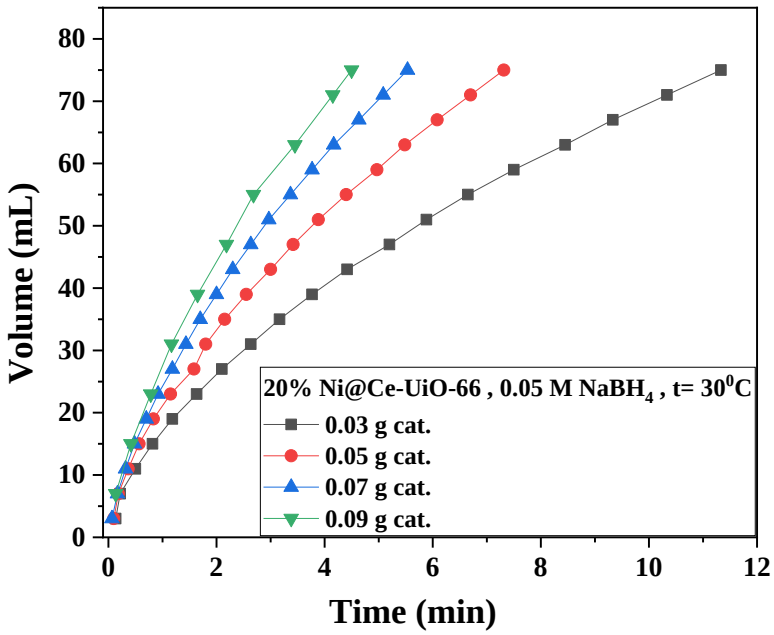

Fig. 5: The effect of 20% Ni@Ce-UiO-66 loading on hydrogen generation via $NaBH_4$ hydrolysis.

2.2. Effect of $NaBH_4$ concentration

The hydrogen production efficiency was evaluated across various $NaBH_4$ concentrations (0.05-0.11 *M*) using 0.03g of catalyst at 30°C. Fig. 6 presents the time-dependent hydrogen evolution regimes that revealing two key trends: (1) both the total hydrogen yield and production rate increased proportionally with $NaBH_4$ concentration, and (2) the reaction completion time significantly decreased at the concentration of $NaBH_4$ increased.

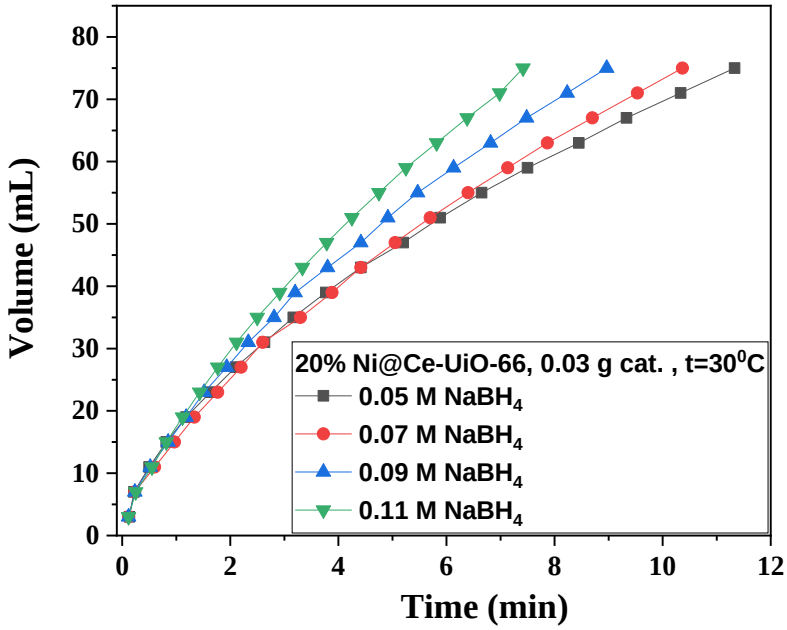

Fig. 6: The influence of different $NaBH_4$ concentrations (0.05 M, 0.07 M, 0.09 M, and 0.11 *M*).

2.3. Effect of reaction temperature

Temperature significantly influences the hydrolysis kinetics in hydrogen production events, as evidenced in Fig. 7. The experimental data reveal a direct correlation between reaction temperature and hydrogen evolution rate during $NaBH_4$ hydrolysis. This temperature dependence originates from the enhancement of molecular kinetic energy at elevated temperatures, which accelerates the reaction dynamics. The results conclusively establish reaction temperature as a critical parameter governing hydrogen generation rates in this context.

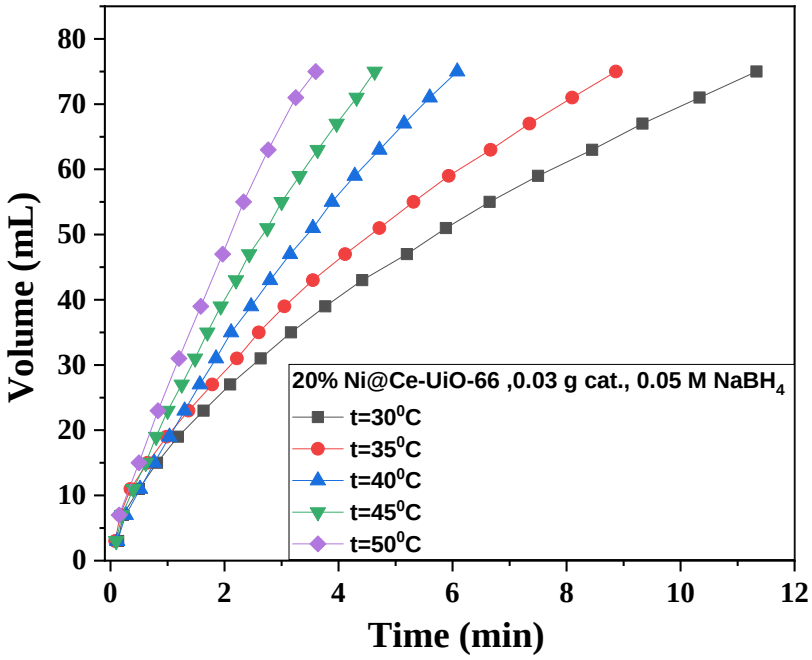

Fig. 7: Hydrogen generation from $NaBH_4$ via 20% Ni@Ce-UiO-66 at various reaction temperatures of 30, 35, 40, 45, and 50 °C.

3. Catalytic dehydrogenation kinetic and thermodynamic parameters

Kinetic and thermodynamic analysis of the catalytic dehydrogenation process was performed by transforming the obtained hydrogen volume-time (V_{H_2}–t) data into sodium borohydride concentration-time ([$NaBH_4$]–t) plots. These were subsequently converted to ln(a-x)–t plots (Fig. 8a) to establish the reaction order (n) through iterative analysis. The reaction rate constant (k) was derived from the slope of the linearized ln(a-x)–t relationship. Temperature-dependent rate constants (30-50°C) were further analyzed using the linearized Arrhenius equation (2) to determine the activation parameters.

$$\ln k = \ln A - E_a/RT \quad (2)$$

The kinetic parameters were defined as follows: k represents the reaction rate constant, A denotes the pre-exponential factor, R is the universal gas constant (8.314 J mol^{-1} K^{-1}), and T signifies the absolute temperature. Activation energy (E_a) was also determined from the slope of the linear Arrhenius plot (ln k vs. 1/T) presented in Fig. 8b, exhibiting a value of 47.5 kJ/mol with excellent correlation (R^2 = 0.994). Furthermore, thermodynamic parameters including enthalpy change (ΔH) and entropy change (ΔS) were evaluated using the Eyring equation (3) to characterize the reaction pathway.

$$k = k_B T/h\, e^{\Delta S/R}\, e^{-\Delta H/RT} \quad (3)$$

k represents the reaction rate constant, k_B denotes the Boltzmann constant (1.381×10^{-23} $J \cdot K^{-1}$), and h is Planck's constant (6.626×10^{-34} $J \cdot s$). The fundamental thermodynamic relationship governing the process were interelated by Equation (4):

$$\Delta G = \Delta H - T\Delta S \quad (4)$$

where ΔS is the activation entropy, ΔG signifies the Gibbs free energy of activation, T is the absolute temperature, and ΔH represents the enthalpy change for $NaBH_4$ dehydrogenation (-212.1 $kJ \cdot mol^{-1}$).

The thermodynamic functions presented in Table. 2 demonstrate the negative sign for both ΔG and ΔH, accompanied by a positive ΔS values. These results collectively confirm the thermodynamic favorability of $NaBH_4$ catalytic dehydrogenation over the Ni@Ce-UiO-66 catalyst system.

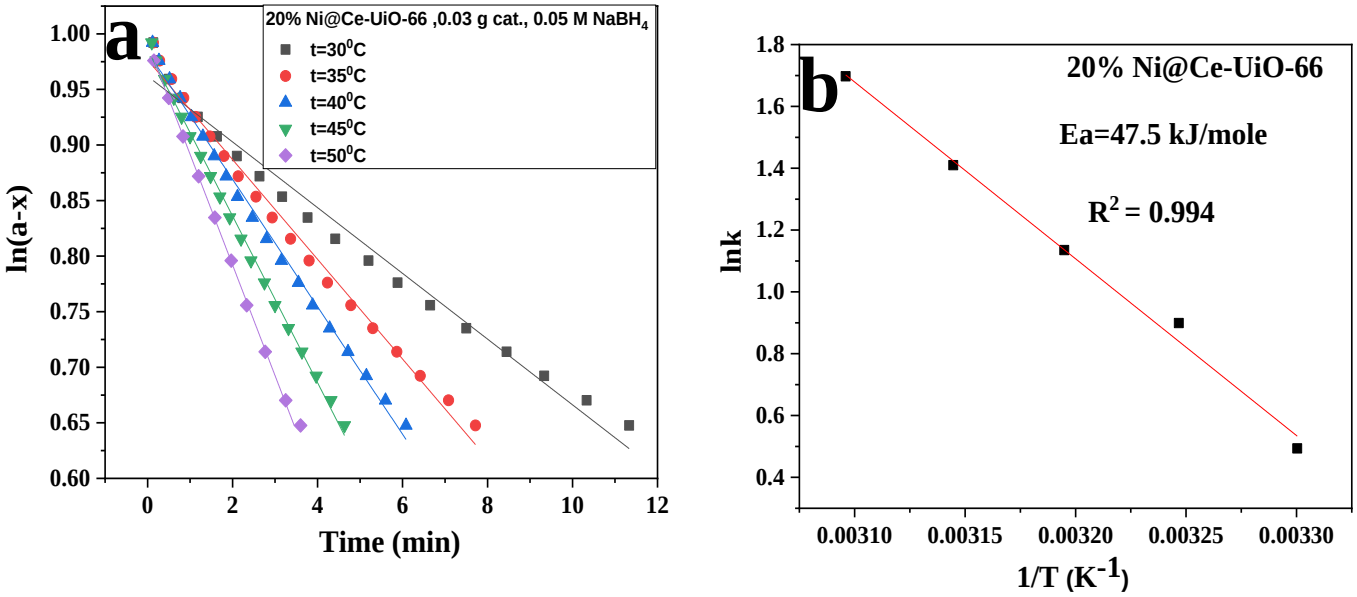

Fig. 8: a) ln (a-x) versus time plots constructed for the $NaBH_4$ dehydrogenation reaction on Ni@Ce-UiO-66 at different reaction temperatures (30-50 ^{0}C), b) Arrhenius plots (ln k versus 1/T) constructed for the $NaBH_4$ dehydrogenation reaction on Ni@Ce-UiO-66.

Table 2: The rate constant, activation energy, enthalpy change, the entropy and free energy of activation for the catalytic $NaBH_4$ dehydrogenation reaction.

T (^{0}K)	k (min^{-1})	Ea ($kJ.mol^{-1}$)	ΔH ($kJ.mol^{-1}$)	ΔS ($kJ.mol^{-1}$)	ΔG ($kJ.mol^{-1}$)
303	0.03	47.5	-212.1	0.97	-83.0
308	0.045			0.96	-83.4
313	0.057			0.947	-84.4
318	0.075			0.930	-84.9
323	0.10			0.92	-85.5

4. Reaction mechanism

Regarding the $NaBH_4$ hydrolysis literature [37], our proposed mechanism explores the following three critical stages: (i) reactant adsorption takes place on Ni^{2+}sites within the MOF's nanochannels, (ii) Ni^{2+} mediated B-H bond activation via electron withdrawal, and (iii) stepwise protonation through a $BH_3(OH)^-$ intermediate that undergoes three hydrolytic conversions (each producing H_2) until metaborate formation completion. The MOF architecture serves dual roles: ensuring high dispersion of Ni^{2+} active sites meanwhile structurally templating the reaction sequence for controlled hydrogen evolution kinetics essential in storage systems.

5. Catalyst recyclability

Catalyst recyclability was systematically evaluated through multiple reaction cycles (Fig. 9). The experimental data demonstrate that 20% Ni@Ce-UiO-66 maintains consistent catalytic activity across four consecutive runs, indicating exceptional recyclability. This performance stability suggests the material's robust structural integrity, with no significant degradation or morphological alterations that would compromise its functionality. The observed reusability of 20% Ni@Ce-UiO-66 highlights its potential for extended application in catalytic processes, offering both economic and environmental advantages through reduced material consumption and minimized waste generation. These findings underscore the catalyst's contribution to sustainable chemical processes.

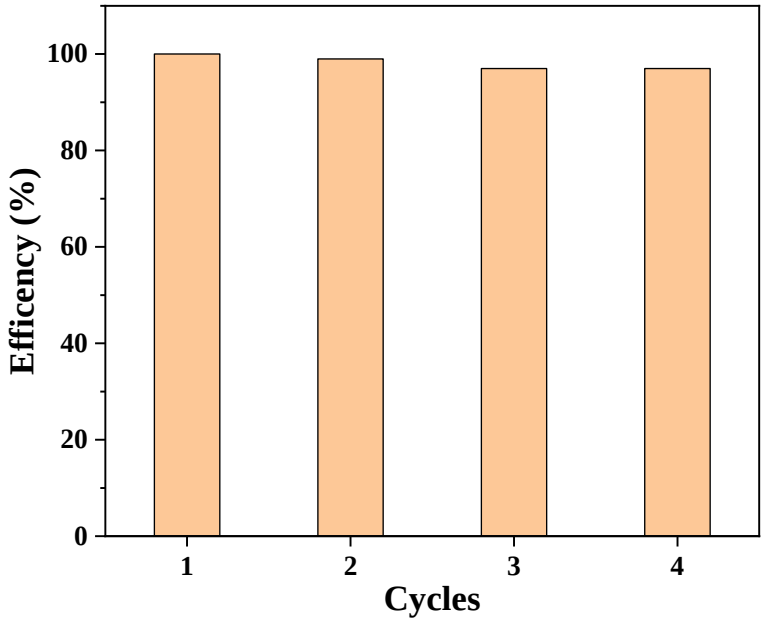

Fig. 9: Recyclability effect on the performance of 20% Ni@Ce-UiO-66 catalyst.

Table 3 presents a comparative analysis of hydrogen generation rates (HGR) between our developed catalysts and previously reported systems. Notably, the 20% Ni@Ce-UiO-66 catalyst demonstrates superior HGR performance when benchmarked

against reference catalysts including Ni [38], WSC-Ni [39], NiB/$NiFe_2O_4$ [40], Ce-UiO-66, and 15% SO_4 /Ce-UiO-66 [41].

Table 3: HGR values measured using our present catalysts and literature-reported ones.

Catalyst	Catalyst wt.	Reaction conditions	HGR ($mL.min^{-1}.g^{-1}$)	Ref.
Ni	75%	14 wt% $NaBH_4$، 30° C	96.3	[38]
WSC-Ni	100 mg	$NaBH_4$ (1.0 g/L), 30°C	130	[39]
NiB/$NiFe_2O_4$	100 mg	$NaBH_4$ (5 wt.%); NaOH (5 wt.%), 25°C	300	[40]
Ce-UiO-66	50 mg	0.05 M $NaBH_4$, 30 ^{0}C	97.4	[41]
15% SO_4/Ce-UiO-66	50 mg	0.05 M $NaBH_4$, 30 ^{0}C	163.1	[41]
20 % Ni@Ce-UiO-66	50 mg	0.05 M $NaBH_4$, 30 ^{0}C	205.5	This study
20 % Ni@Ce-UiO-66	30 mg	0.11 M $NaBH_4$, 30 ^{0}C	336.9	This study
20 % Ni@Ce-UiO-66	30 mg	0.05 M $NaBH_4$, 30 ^{0}C	222.8	This study
20% Ni@Ce-UiO-66	30 mg	0.05 M $NaBH_4$, 35^{0}C	284	This study
20% Ni@Ce-UiO-66	30 mg	0.05 M $NaBH_4$, 40 ^{0}C	409.8	This study
20% Ni@Ce-UiO-66	30 mg	0.05 M $NaBH_4$, 45 ^{0}C	540	This study
20% Ni@Ce-UiO-66	30 mg	0.05 M $NaBH_4$, 50 ^{0}C	694	This study

CONCLUSIONS

Ni@Ce-UiO-66 catalysts were synthesized via wet impregnation by loading Ce-UiO-66 with 10-20 wt.% nickel nitrate hexahydrate ($Ni(NO_3)_2 \cdot 6H_2O$). XRD, FTIR, and N_2 adsorption techniques were employed to characterize the synthesized catalysts prior to testing their catalytic efficiency via sodium borohydride dehydrogenation. These catalysts prevailed excellent efficiency, reduction of reaction time completion, minimizing the catalyst usage, and low metal leaching. A superior hydrogen evolution rate of 694 mL min^{-1} g^{-1} was observed for 20% Ni@Ce-UiO-66 under optimized conditions (50°C, 30 mg catalyst, 50 mM $NaBH_4$). The reaction kinetics followed first-order behavior at reduced borohydride concentrations, exhibiting an activation energy barrier of 47.5 kJ mol^{-1}.Thermodynamic data confirm the spontaneity, feasibility and exothermicity of the hydrolysis reaction. The materials also retained high catalytic activity over four cycles, demonstrating excellent recyclability, making them suitable for scalable energy applications.

Acknowledgment

This work was financially supported by Assiut University, Egypt.

REFERENCES

[1] D.X. Liu, Y.T. Zhou, Y.F. Zhu, Z.Y. Chen, J.M. Yan, Q. Jiang, Tri-metallic aupdir nanoalloy towards efficient hydrogen generation from formic acid, Appl. Catal. B-Environ. 309 (2022) 121228.

[2] M. Aziz, A. Darmawan, F.B. Juangsa, Hydrogen production from biomasses and wastes: A technological review, Int. J. Hyrogen Energy 46 (2021) 33756–33781.

[3] T. Wang, L. Tao, X. Zhu, C. Chen, W. Chen, S. Du, Y. Zhou, B. Zhou, D. Wang, C. Xie, P. Long, W. Li, Y. Wang, R. Chen, Y. Zou, X.Z. Fu, Y. Li, X. Duan, S.Wang, Combined anodic and cathodic hydrogen production from aldehyde oxidation and hydrogen evolution reaction, Nat. Catal. 5 (2022) 67–73.

[4] S. Jing, L. Zhang, L. Luo, J. Lu ,S. Yun ,P.K. Shen, P. Tsiakaras , N-Doped Porous Molybdenum Carbide Nanobelts as Efficient Catalysts for Hydrogen Evolution Reaction, Appl. Catal. 224 (2018) 533-540.

[5] R. Kothari, D. Buddhi, R.L. Sawhney, Comparison of environmental and economic aspects of various hydrogen production methods, Renew. Sustain. Energy Rev. 12 (2008) 553–563.

[6] A. Flamos, P.G. Georgallis, H. Doukas, J. Psarras, Using biomass to achieve European Union energy targets-a review of biomass status, potential, and supporting policies, Int. J. Green Energy 8 (2011) 411–428 .

[7] E. Gürtekin, Biological Hydrogen Production Methods, 2Nd Int. Symp. Environ. Moral. C (2014) 463–471.

[8] S. Liu, J. Zhu, M. Chen, W. Xin, Z. Yang, L. Kong, Hydrogen production via

catalytic pyrolysis of biomass in a two-stage fixed bed reactor system, Int. J. Hydrogen Energy 39(25) (2014) 13128–13135.

[9] M. Farrag, Ultrasmall bimetallic Ru-Co alloy nanoclusters immobilized in amino-functionalized UiO-66 and N-doped carbonaceous zirconium oxide nanocomposite for hydrogen generation, J. Alloys Compd. 920 (2022) 165893.

[10] M. Farrag, G.A.M. Ali, Hydrogen generation of single alloy Pd/Pt quantum dots over Co3O4 nanoparticles via the hydrolysis of sodium borohydride at room temperature, Sci. Rep. 12 (2022) 17040.

[11] A. Chinnappan, J. M. C. Puguan, W. J. Chung, H. Kim, Hydrogen generation from the hydrolysis of sodium borohydride using chemically modified multiwalled carbon nanotubes with pyridinium based ionic liquid and decorated with highly dispersed Mn nanoparticles, J. Power Sources 293 (2015) 429-436.

[12] O. Sahin, D. Kılınc, C. Saka, Hydrogen generation from hydrolysis of sodium borohydride with a novel palladium metal complex catalyst, J. Energy Inst. 89 (2016) 182-189.

[13] G. Guella, C. Zanchetta, B. Patton, A. Miotello, New insights on the mechanism of palladium-catalyzed hydrolysis of sodium borohydride from 11B NMR measurements. J. Phys. Chem. B 110 (2006) 17024-17033.

[14] S. C. Amendola, S. L. Sharp-Goldman, M. S. Janjua, N. C. Spencer, M. T. Kelly, P. J. Petillo, M. Binder, A safe, portable, hydrogen gas generator using aqueous borohydride solution and Ru catalyst. Int. J. Hydrogen Energy 25 (2000) 969-975.

[15] L. Schlapbach, A. Zuttel, Hydrogen-storage materials for mobile applications, Nature 414 (2001) 353-358.

[16] N. Sahiner, A. O. Yasar, N. Aktas, Dicationic poly(4-vinyl pyridinium) ionic liquid capsules as template for Co nanoparticle preparation and H2 production from hydrolysis of $NaBH_4$. J. Ind. Eng. Chem. 23 (2015)100-108.

[17] Y. Kojima, Y. Kawai, H. Nakanishi, S. Matsumoto, Compressed hydrogen generation using chemical hydride, J. Power Sources 135 (2004) 36-41.

[18] D. Kilinc, C. Saka, O. Sahin, Hydrogen generation from catalytic hydrolysis of sodium borohydride by a novel Co(II)- Cu(II) based complex catalyst, J Power Sources

217 (2012) 256-261.

[19] O. Sahin, D. Kilinc, C. Saka, Hydrogen production by catalytic hydrolysis of sodium borohydride with a bimetallic solidstate Co-Fe complex catalyst. Separ. Sci. Technol. 50 (2015) 2051-2059.

[20] S. Eug_enio, U. B. Demirci, T. M. Silva, M. J. Carmezim, M. F. Montemor. Copper-cobalt foams as active and stable catalysts for hydrogen release by hydrolysis of sodium borohydride, 41 (2016) 8438-8448.

[21] D. Kilinc, O. Sahin, Synthesis of polymer supported Ni (II) - Schiff Base complex and its usage as a catalyst in sodium borohydride hydrolysis. Int. J. Hydrogen Energy 43 (2018) 10717-10727.

[22] P. Tignol, U. B. Demirci, Nickel-based catalysts for hydrogen evolution by hydrolysis of sodium borohydride: from structured nickel hydrazine nitrate complexes to reduced counterparts, Int. J. Hydrogen Energy 44 (2019)14207-14216.

[23] H.N. Abdelhamid, Z. Huang, A.M. El-Zohry, H. Zheng, X. Zou, A Fast and Scalable Approach for Synthesis of Hierarchical Porous Zeolitic Imidazolate Frameworks and One-Pot Encapsulation of Target Molecules, Inorg. Chem. 56(15) (2017) 9139–9146.

[24] Y. Yang, K. Chen , J.Z. Lin, Y. Zhou ,Q.Y. Liu, C. Hang , H.N. Abdelhamid, Z.Q. Zhang, H. Chen ,A Zn-MOF constructed from electron-rich π-conjugated ligands with an interpenetrated graphene-like net as an efficient nitroaromatic sensor, RSC Adv. 6 (2016) 45475–45481.

[25] H.N. Abdelhamid , X. Zou, Template-free and room temperature synthesis of hierarchical porous zeolitic imidazolate framework nanoparticles and their dye and CO_2 sorption, Green Chem. 20 (2018) 1074–1084.

[26] A.F. Abdel-Magied, H.N. Abdelhamid, R.M. Ashour, X. Zou, K. Forsberg, Hierarchical porous zeolitic imidazolate frameworks nanoparticles for efficient adsorption of rare-earth elements, Microporous Mesoporous Mater. 278 (2019) 175–184.

[27] Z. Chen, S. L. Hanna, L. R. Redfern, D. Alezi, T. Islamoglu, and O. K. Farha, Reticular chemistry in the rational synthesis of functional zirconium cluster-based MOFs, Coord. Chem. Rev. 386 (2019) 32–49.

[28] H.N. Abdelhamid, Surfactant assisted synthesis of hierarchical porous metal-organic frameworks nanosheets, Nanotechnol. 30 (2019) 435601.

[29] J.M. Yassin, A.M. Taddesse, M.S. Sanchez, Room temperature synthesis of high-quality Ce (IV) -based MOFs in water, Microporous Mesoporous Mater. 324 (2021) 111303.

[30] F.T. Alshorifi, D.E. Tobbala, S.M. El-Bahy, M.A. Nassan, and R.S. Salama, The role of phosphotungstic acid in enhancing the catalytic performance of UiO-66 (Zr) and its applications as an efficient solid acid catalyst for coumarins and dihydropyrimidinones synthesis, Catal. Commun. 169 (2022) 106479.

[31] X. Liao, X. Wang, F. Wang, Y. Yao, S. Lu, Ligand Modified Metal Organic Framework UiO-66: A Highly Efficient and Stable Catalyst for Oxidative Desulfurization, J Inorg. Organomet. Polym. Mater. 31 (2021) 756–762.

[32] F. Khosravi, M. Gholinejad, J.M. Sansano, R. Luque, Bimetallic Fe–Cu metal organic frameworks for room temperature catalysis, Appl. Organomet. Chem. 36 (2022) 6749.

[33] S. Subudhi, G. Swain, S.P. Tripathy, K. Parida, UiO-66-NH_2 Metal-Organic Frameworks with Embedded MoS_2Nanoflakes for Visible-Light-Mediated H_2 and O_2 Evolution, Inorg. Chem. 59(14) (2020) 9824–9837.

[34] A. Raghi, K. Ghani, M. Jafari, Modification of UiO-66 for removal of uranyl ion from aqueous solution by immobilization of tributyl phosphate, J. Chem. Sci. 133 (2021) 14.

[35] A.S. Elsherbiny, A. Rady, R.M. Abdelhameed, A.H. Gemeay, Efficiency and selectivity of cost-effective Zn-MOF for dye removal, kinetic and thermodynamic approach, Environ. Sci. Pollut. Res. 30 (2023) 106860–106875.

[36] N. Riezzati, Y.K. Krisnandi, A. Zulys, Metal organic frameworks of lanthanum and iron using BDC linker as catalysts for glucose conversion into 5-hydroxymethylfurfural (5-HMF), IOP Conf. Ser.: Mater. Sci. Eng. 902 (2020) 012044.

[37] U.B. Demirci, P. Miele, Reaction mechanisms of the hydrolysis of sodium borohydride: a discussion focusing on cobalt-based catalysts, C. R. Chim. 17 (2014) 707–716.

[38] J.– H. Kim, K.– T. Kim, Y.–M. Kang, H. S. Kim, M.–S. Song, Y.–J. Lee, et al, Study on degradation of filamentary Ni catalyst on hydrolysis of sodium borohydride, J. Alloys Compd. 379 (2004) 222-7.

[39] J. Ding, Q. Li, Y. Su, Q. Yue, B. Gao, W. Zhou, Preparation and catalytic activity of wheat straw cellulose based hydrogel-nanometal composites for hydrogen generation from $NaBH_4$ hydrolysis**,** Int. J. Hydrogen Energy. 43 (2018) 9978–9987.

[40] Z. Liang, Q. Li, F. Li, S. Zhao, X. Xia, Hydrogen generation from hydrolysis of $NaBH_4$ based on high stable NiB/$NiFe_2O_4$ catalyst Int. J. Hydrogen Energy. 42 (2017) 3971–3980.

[41] A. Abdo Hassan, M. Farrag, R. M. Gabr, Synthesis and characterization of functionalized cerium and zirconium metal-organic frameworks as novel solid acid catalysts for hydrogen generation, Egypt. J. Chem. 68(5) (2025) 179 – 192.